JOURNAL OF MAGNETIC RESONANCE **129,** 67–73 (1997)
ARTICLE NO. MN971246

Three-Dimensional Maximum-Quantum Correlation HMQC NMR Spectroscopy (3D MAXY-HMQC)

Maili Liu,*,† Xi-An Mao,* Chaohui Ye,* Jeremy K. Nicholson,‡ and John C. Lindon‡,[1]

*Laboratory of Magnetic Resonance and Atomic and Molecular Physics, Wuhan Institute of Physics and Mathematics, The Chinese Academy of Science, Wuhan 430071 People's Republic of China; †Instrumental Analytical Research Centre, Northwest University, Xi'an 710069, People's Republic of China; and ‡Department of Chemistry, Birkbeck College, University of London, Gordon House, 29 Gordon Square, London WC1H 0PP, United Kingdom

Received February 17, 1997; revised July 30, 1997

The extension of two-dimensional maximum-quantum correlation spectroscopy (2D MAXY NMR), which can be used to simplify complex NMR spectra, to three dimensions (3D) is described. A new pulse sequence for 3D MAXY-HMQC is presented and exemplified using the steroid drug dexamethasone. The sensitivity and coherence transfer efficiency of the MAXY NMR approach has also been assessed in relation to other HMQC- and HSQC-based 3D methods. © 1997 Academic Press

INTRODUCTION

In one- and two-dimensional maximum-quantum correlation NMR spectroscopy (1D and 2D MAXY NMR), the maximum-quantum coherence has been used either as a filter or as a modulator to provide the second frequency dimension, or both (*1–5*). This approach provides an option of distinguishing CH_n groups either by their precession frequencies or by selective detection using phase cycling or pulsed field gradients (PFG). Application of MAXY methods for assignment of NMR resonances has been demonstrated for medium-sized molecules such as dexamethasone (*1, 2*) and sodium taurocholate (*3, 4*). The peptide neurotensin, consisting of 13 residues, was chosen as an example to show that the approach can be used as an alternative to ^{13}C and ^{15}N labeling methods, and the results have been compared with INEPT- and DEPT-based two-dimensional experiments (*5*). Other examples where MAXY NMR has been used include complex biofluids (human seminal fluid and blood plasma) where the new methods have been used to provide an augmented list of resonance assignments for endogenous metabolites, especially in the very crowded region of the spectrum between δ3.0 and δ4.5 where there are many overlapping signals from sugars and polyols (*1, 3*).

[1] To whom correspondence should be addressed. Fax: +44-171-380-7464.

Three-dimensional (3D) NMR experiments, such as 3D NOESY-HMQC/HSQC (*6–10*), 3D TOCSY-HMQC/HSQC (*7–11*), 3D NOESY-TOCSY (*12*), and a number of derivatives (*12–19*), have been used extensively for resonance assignment and structural determination of macromolecules where the signal overlap in two-dimensional (2D) spectra of larger proteins or nucleic acids is too extreme (*20*). It is possible to insert a second variable delay into the 2D MAXY pulse sequences to generate 3D NMR experiments. This new dimension could cover proton or heteronuclear chemical shifts or spin–spin coupling constant splittings leading to 3D experiments such as 3D MAXY-TOCSY, 3D MAXY-HMQC, and 3D MAXY-JRES NMR spectroscopy. In this paper, the pulse sequence of 3D MAXY-HMQC is described. The sensitivity and coherence transfer efficiency of the method are discussed and compared with other HSQC- and HMQC-based methods (*21–24*).

3D MAXY-HMQC PULSE SEQUENCE AND THEORY

Figure 1 shows a 3D MAXY-HMQC pulse sequence, which is based upon the 2D MAXY experiment (*2*) and has an additional variable delay (t_2) inserted before the point where heteronuclear zero- and double-quantum coherence are converted to proton single-quantum coherence. The coherence transfer pathways for different spin systems (SI_n) are given in the figure. These are shown with quantum levels on the right-hand side and coherence levels for proton (I) and carbon (S) are given separately. The entire process can be clearly described using the product operator formalism (*25*).

The precession periods in the 3D pulse sequence can be classified into two kinds, one being for heteronuclear coupling precession during Δ and the other for chemical shift precession during variable times t_1 and t_2. It can be seen from Fig. 1 that all of the Δ delays are symmetric about the 180° pulses and thus the chemical shifts will be refocused. The evolution of the J coupling can be written as (*25*)

1090-7807/97 $25.00

$$I_{x,y} \xrightarrow{2\pi J_{IS} I_z S_z} I_{x,y}\cos(\pi J_{IS}\Delta) \pm 2I_{y,x}S_z\sin(\pi J_{IS}\delta) \quad [1a]$$

$$2I_{x,y}S_z \xrightarrow{2\pi J_{IS} I_z S_z} 2I_{x,y}S_z\cos(\pi J_{IS}\Delta) \pm I_{y,x}\sin(\pi J_{IS}\Delta). \quad [1b]$$

When the delay Δ is set to $1/(2^1J_{IS})$, only the last terms exist as $(\pm 2I_{y,x}S_z)$ and $(\pm I_{y,x})$, respectively. It is possible to ignore the other terms by making the assumptions that all of the one-bond heteronuclear coupling constants have the same value, and that values of the long-range heteronuclear, ${}^nJ_{IS}$, and homonuclear, J_{II}, coupling constants are much smaller than the one-bond heteronuclear coupling constants.

The two protons of an SI_2 group are distinguished as they are often chemically and magnetically nonequivalent. The $180^\circ_y(S)$ pulse in the middle of the first increment time (t_1) refocuses the spin S (^{13}C) chemical shifts and heteronuclear couplings (in this case long-range heteronuclear couplings); thus only spin I (^1H) chemical shifts precess at their maximum-quantum frequencies. If only the I-spin operators are considered, the coherence quantum levels are single quantum (SQ) for SI groups, pure double quantum (DQ) for SI_2 groups, and triple and single quantum (TQ & SQ) for SI_3 groups, respectively. The observable terms after the first variable time (t_1) may be written as

$$\begin{aligned} &-2I_xS_y\cos(2\pi\delta_i t_1)\Pi\cos(\pi J_{ij}t_1) && (SI)\\ &+4[I_{1x}I_{2y} + I_{1y}I_{2x}]S_x\cos(2\pi(\delta_{1i} + \delta_{2i})t_1)\Pi\cos(\pi J_{1j}t_1)\cos(\pi J_{2j}t_1) && (SI_2)\\ &+6I_xI_yI_yS_y[3\cos(6\pi\delta_i t_1) + \cos(2\pi\delta_i t_1)]\Pi\cos^3(\pi J_{ij}t_1) && (SI_3), \end{aligned} \quad [3]$$

The I-spin single-quantum coherence ($-I_y$) produced by the first $90^\circ_x(I)$ pulse involves the heteronuclear magnetization through the $\pi\,{}^1J_{IS}\Delta 2I_zS_z$ operator during the first delay to yield $2I_xS_z$ which is then converted to heteronuclear zero- and double-quantum coherence by the first $90^\circ_x(S)$ pulse as $+2I_xS_y$. During the next delay, magnetization of protons in SI_2 and SI_3 groups are evolved by the $\pi\,{}^1J_{IS}\Delta 2I_zS_z$ operator and finally excited to their heteronuclear maximum-quantum level by the second $90^\circ_x(I)$ pulse, which also converts the single-quantum coherence of any I spin not bonded to an S spin (for example, expressed here for ^1H and ^{12}C as XH_n) to z magnetization. The preparation process can be summarized as where δ_i represents the proton chemical shifts and $\Pi\cos(2\pi J_{ij}t_1)$ represents the passive $^1H-{}^1H$ couplings evolving during t_1. It is notable that while the precession frequency for an SI group is the spin I single-quantum frequency, that for an SI_2 group is the sum of the two I-spin frequencies corresponding to spin I double-quantum coherence. There are two precession frequencies for SI_3 groups, spin I triple- and single-quantum coherence with a ratio of 3:1. The third $90^\circ_{-x}(I)$ pulse followed by a delay $\Delta\,(1/2J)$ converts the maximum-quantum coherence to heteronuclear double- and zero-quantum coherence:

$$\begin{aligned} &-2I_xS_y\cos(2\pi\delta_i t_1)\Pi\cos(\pi J_{ij}t_1) && (SI)\\ &-2[I_{1x} + I_{2x}]S_y\cos(2\pi(\delta_{1i} + \delta_{2i})t_1)\,\Pi\cos(\pi J_{1j}t_1)\cos(\pi J_{2j}t_1) && (SI_2)\\ &-3/2I_xS_y[3\cos(6\pi\delta_i t_1) + \cos(2\pi\delta_i t_1)]\Pi\cos^3(\pi J_{ij}t_1) && (SI_3). \end{aligned} \quad [4]$$

The geminal H–H coupling of nonequivalent CH_2 protons needs to be considered explicitly. During t_1, the MAXY period, both spins of such groups evolve to the double-

$$\begin{array}{lll} SI_n + I_z & \xrightarrow{90^\circ_x(I)} -I_y & \xrightarrow{-180^\circ_x(I)90^\circ_x(S)} -2I_xS_y \\ XH_n + I_z & -I_y & +I_y \end{array}$$

$$\xrightarrow{-90^\circ_x(I)}$$

$$\begin{aligned} &= -2I_xS_y && (SI)\\ &= -4[I_{1x}I_{2y} + I_{1y}I_{2x}]S_x && (SI_2)\\ &= +3[8I_xI_yI_y]S_y && (SI_3)\\ &= -I_z && (XH_n). \end{aligned} \quad [2]$$

quantum coherence and therefore the coupling has no effect. However, during t_2, the HMQC period, some magnetization transfer is possible but this will not affect the HMQC correlation.

From the starting point of the second increment time (t_2), the pulse sequence is similar to the conventional HMQC (*23, 24*), where S-spin chemical shift precesses. The observable terms at the beginning of the acquisition time (t_3) are given by

$$\begin{aligned} &-I_y\cos(2\pi\delta_s t_2)\cos(2\pi\delta_i t_1)\Pi\cos(\pi J_{ij}t_1)\Pi\cos(\pi J_{ij}t_2) \quad (\mathrm{SI}) \\ &-I_{1,2y}\cos(2\pi\delta_s t_2)\cos(2\pi(\delta_{1i}+\delta_{2i})t_1)\Pi\cos(\pi J_{1j}t_1)\cos(\pi J_{2j}t_1)\Pi\cos(\pi J_{(1,2)j}t_2) \quad (\mathrm{SI}_2) \\ &-3/4I_y\cos(2\pi\delta_s t_2)[3\cos(6\pi\delta_i t_1)+\cos(2\pi\delta_i t_1)]\Pi\cos^3(\pi J_{ij}t_1)\Pi\cos(\pi J_{ij}t_2) \quad (\mathrm{SI}_3). \end{aligned} \qquad [5]$$

All terms in Eq. [5] have in-phase absorption lineshapes in F_1 (spin I maximum-quantum frequencies), F_2 (spin S single-quantum frequencies), and F_3 (spin I single-quantum frequencies, detection) dimensions and this should be useful for the analysis of spectra of complex mixtures such as biofluids and macromolecules like peptides and proteins. The experiment can be carried out in phase sensitive mode using the TPPI scheme (*26*) for the MAXY part with 90° phase shifts on the first three I nucleus pulses. Also, either the TPPI scheme with a 90° phase shift on the first 90° S pulse or the STATES method (*27*) can be used for the HMQC part of the sequence. In previous studies using MAXY NMR (*1–4*), it was possible to use magnetic field gradients for coherence selection. It is possible to use the same method in the three-dimensional experiment in exactly the same fashion. However, the loss of sensitivity should be considered.

EXPERIMENTAL

The test sample was dexamethasone (Sigma Chem. Co., Poole, UK) at a concentration of 30 mg, in 0.5 ml DMSO-d_6 (Aldrich Chem. Co., Gillingham, UK). The structure and the numbering system for dexamethasone is given as below:

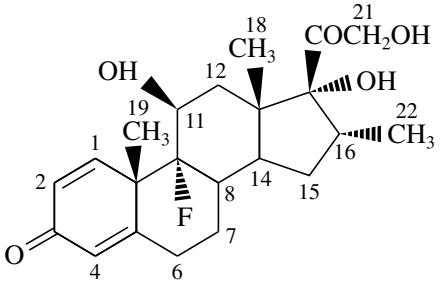

A 3D MAXY-HMQC experiment was carried out on a Bruker AMX600 instrument operating at 600.13 and 150.9 MHz for ^{1}H and ^{13}C, respectively. The delay (Δ) was 3.75 ms corresponding to a one-bond ^{13}C–^{1}H coupling constant of 135 Hz. The spectrum widths were 24 ppm in F_1 (MAXY), 160 ppm in F_2 (HMQC), and 8 ppm in F_3. Twenty-four transients were acquired into 1024 data points with 128 increments in F_1 and 64 increments in F_2. A sine-bell window function was applied in all three dimensions and the F_1 and F_2 dimensions were zero-filled to 256 data points before Fourier transformation to give a data matrix of 256 × 256 × 1024. Linear prediction was used in the F_1 and F_2 dimensions respectively to enhance the resolution and to remove any truncation of the data.

RESULTS

The projections of the 3D MAXY-HMQC spectrum onto the F_1–F_2, F_1–F_3, and F_2–F_3 planes are shown in Figs. 2a,

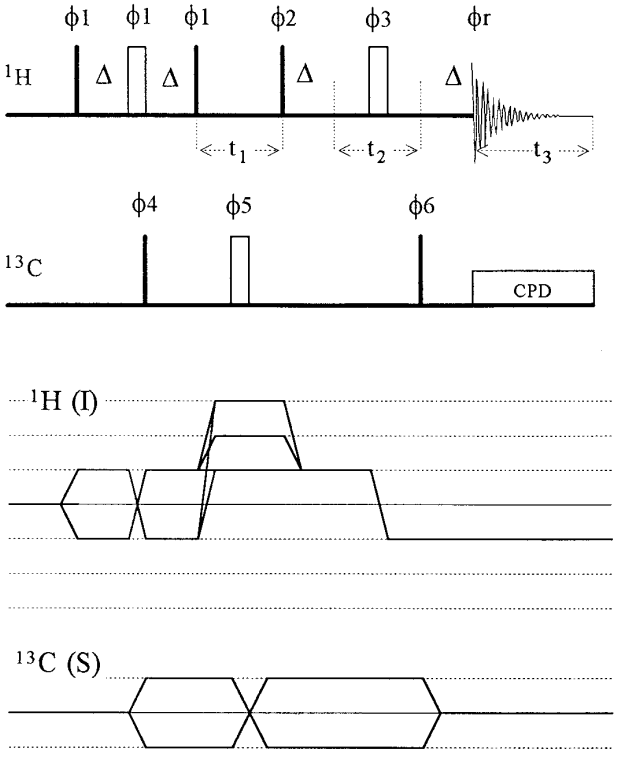

FIG. 1. Pulse sequence and corresponding coherence transfer pathways for the three-dimensional MAXY-HMQC NMR experiment. The phase cycling schemes are $\phi1 = x$; $\phi2 = -x$; $\phi3 = y$; $\phi4 = x, -x$; $\phi5 = y$; $\phi6 = x, x, -x, -x$; $\phi r = x, -x, -x, x$.

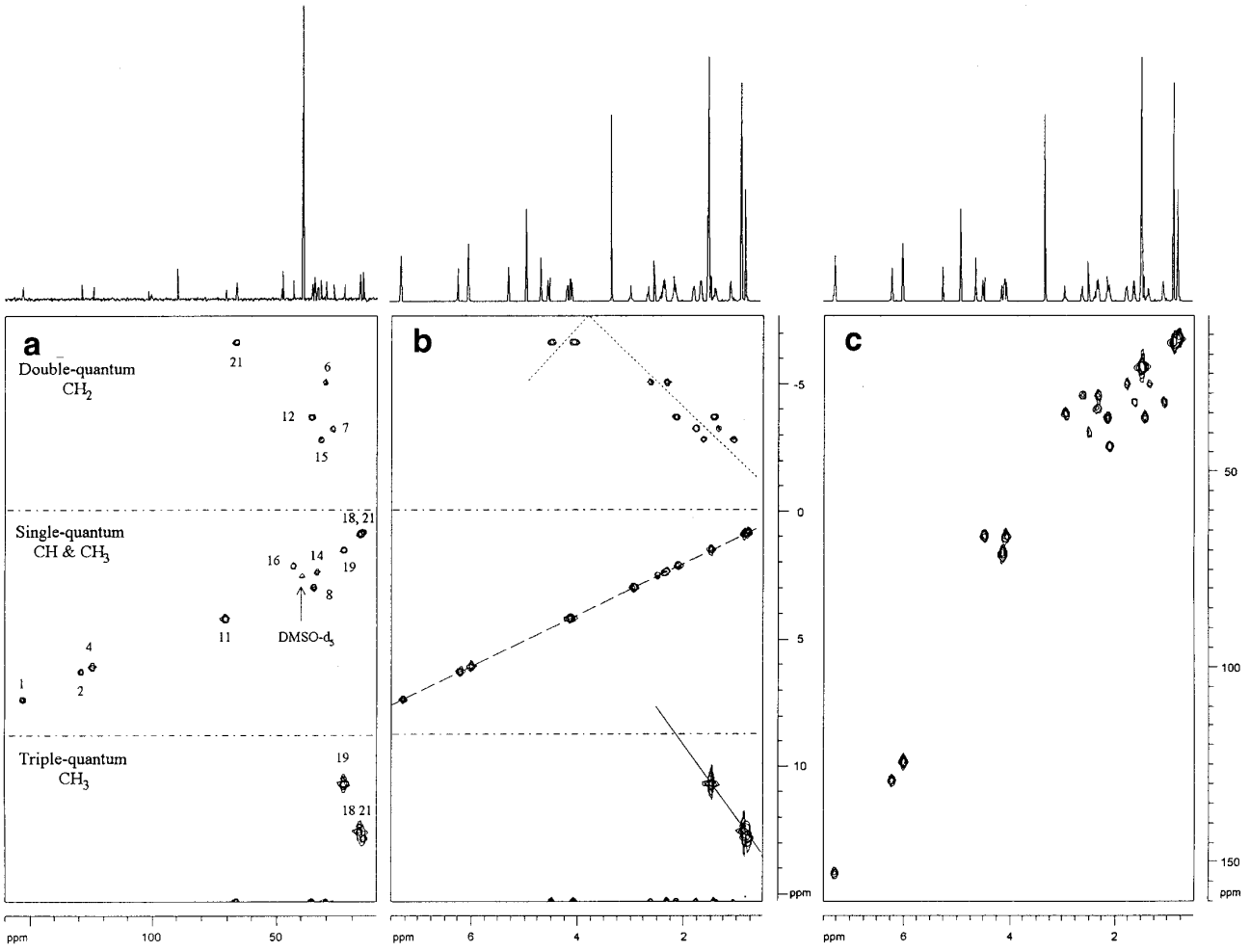

FIG. 2. Projections of the 3D MAXY-HMQC spectrum. (a) Projection onto the F_1–F_2 plane gives a 2D MAXY-HETCOR spectrum with MAXY frequencies in F_1 and normal ^{13}C frequency in F_2; the assignment and spin systems are as given. (b) Projection onto the F_1–F_3 plane gives a 2D MAXY spectrum with MAXY frequencies in F_1 and the normal ^1H frequency in F_2. The diagonals for the triple-, double-, and single-quantum regions are indicated by solid, dotted, and dashed lines, respectively. (c) Projection onto the F_2–F_3 plane gives a 2D HMQC spectrum with the normal ^{13}C frequency in F_1 and the normal ^1H frequency in F_2.

2b, and 2c, respectively. The spectrum in Fig. 2a has ^1H maximum-quantum and ^{13}C single-quantum frequencies in the F_1 and F_2 dimensions, respectively, which is equivalent to a 2D MAXY-HETCOR spectrum (*4*). The projection onto the F_1–F_3 plane (Fig. 2b) gives rise to a 2D MAXY spectrum (*2*). The projection onto the F_2–F_3 plane (Fig. 2c) is identical to a HMQC spectrum (*23*, *24*). The cross peaks in the F_1 dimension of Figs. 2a and 2b have been separated into three regions and the separation enhances the dispersion compared with the HMQC spectrum in Fig. 2c. The resonances of CH_2 groups appear in the upper part of the spectra with double-quantum frequencies, and the peaks of single-quantum coherences of CH and CH_3 groups are in the middle of the spectra, but signals from the CH_3 groups can be readily distinguished by the presence of triple-quantum peaks in the lower part of the spectrum. It is interesting to notice the cross peaks of CH_2 groups in Fig. 2. Each CH_2 group has a single frequency in the F_1 dimension of the spectra corresponding to the double-quantum frequency in Figs. 2a and 2b and the ^{13}C chemical shift in Fig. 2c, respectively. Although geminal protons give rise to two cross peaks in the F_2 dimension of Figs. 2b and 2c, it is not easy to tell which two are from a CH_2 group straightforwardly because of the possibility of ^{13}C chemical shifts overlapping, particularly in the case of macromolecules and of complex mixture. This is not a problem in Fig. 2b, where the two cross peaks of a CH_2 group appear at equal distance from both sides of the double-quantum diagonal (dotted line). Since it is rare to have two geminal CH_2 groups with identical ^1H and ^{13}C chemical shifts, it is possible to distinguish CH_2 groups not

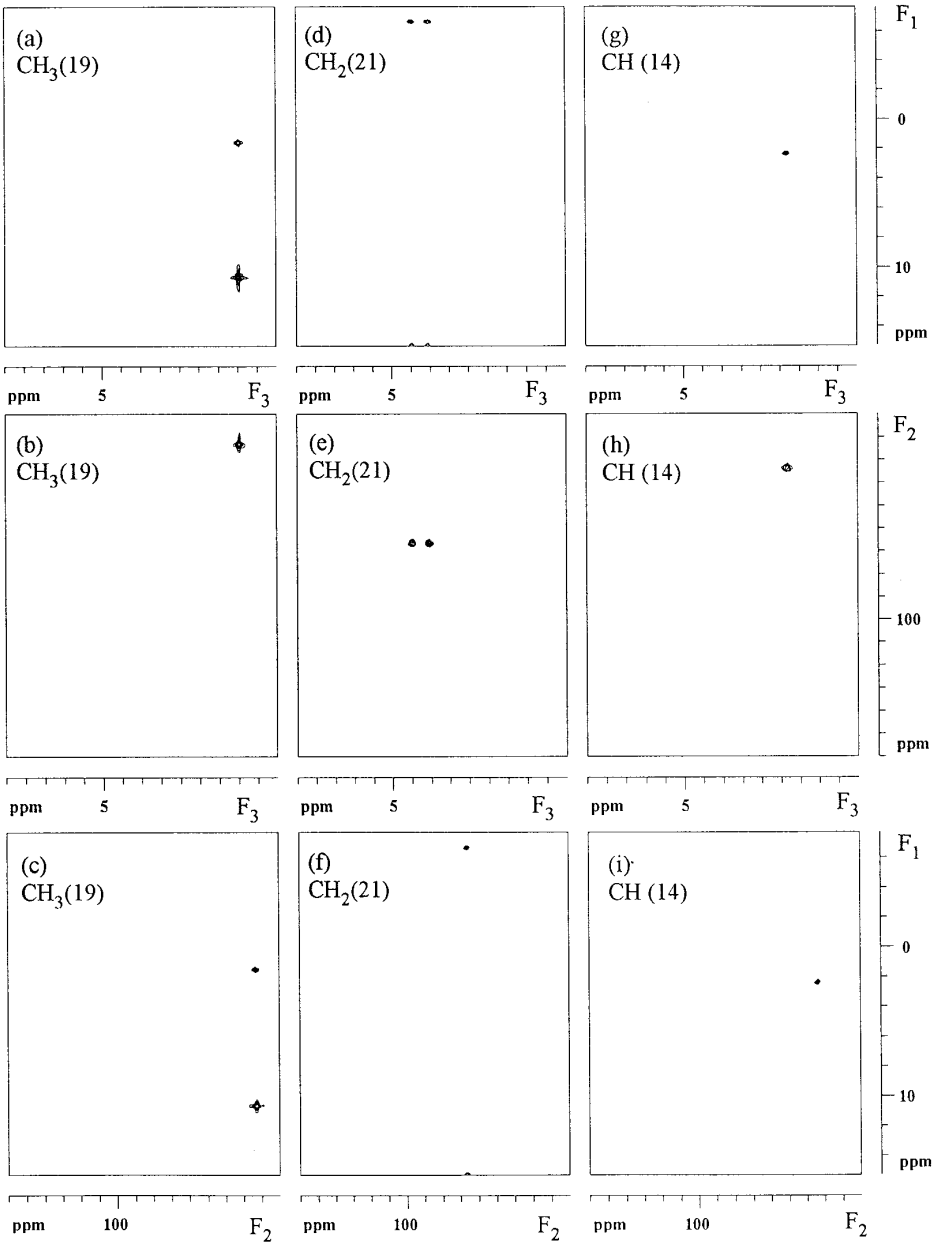

FIG. 3. Planes extracted from the 3D MAXY-HMQC spectrum, with (a, b, c) showing the cross peaks of $CH_3(19)$, (d, e, f) showing the cross peaks of $CH_2(21)$, and (g, h, i) showing the cross peaks of CH(14) from different directions. (a, d, g) are planes along F_2 and correspond to a ^1H 2D MAXY NMR spectrum. (b, e, h) are planes along F_1 and correspond to a $^1H-^{13}C$ 2D HMQC NMR spectrum. (c, f, i) are planes along F_3 and correspond to a 2D MAXY-HECTOR NMR spectrum.

only from the other spin systems (CH and CH_3), but from other CH_2 groups as well. The assignment of the ^1H and ^{13}C resonances of dexamethasone are shown in Fig. 2a.

Figure 3 shows planes extracted from the 3D spectrum, which show cross peaks from $CH_3(19)$ (Figs. 3a, 3b, and 3c), $CH_2(21)$ (Figs. 3d, 3e, and 3f), and CH(14) (Figs. 3g, 3h, and 3i) groups, respectively, where Figs. 3(a, d, g), 3(b, e, h), and 3(c, f, i) are equivalent to selective 2D MAXY, 2D HMQC, and 2D MAXY-HETCOR spectra, respectively, containing only one group in each spectrum. Thus it clearly demonstrates the excellent separation ability of the 3D method.

SENSITIVITY AND COHERENCE TRANSFER EFFICIENCY

For a 3D peak centered at the coordinates (ω_1, ω_2, ω_3), the time-domain signal has the form

$$s(t_1, t_2, t_3) = s^e(t_1, t_2, t_3)\exp(-i\omega_M t_1) \times \exp(-i\omega_S t_2)\exp(-i\omega_I t_3), \quad [6]$$

where ω_M, ω_S, and ω_I represent the transition frequency offsets with respect to the carrier frequency in the maximum-quantum, spin S single-quantum, and detection dimensions, respectively. The envelope function $s^e(t_1, t_2, t_3)$ determines the peak shape in the 3D spectrum:

$$s^e(t_1, t_2, t_3) = R_{cte}(\Delta)\Pi \cos^n(\pi J_{ij} t_1)\Pi \times \cos(\pi J_{ij} t_2) R_2(t_1, t_2, t_3). \quad [7]$$

It can be seen from Eq. [7] that the cross peaks have in-phase absorption lineshapes in all dimensions. In the case of small homonuclear coupling constants and limited increments in the F_1 and F_2 dimensions (this is always true for a 3D experiment), $s^e(t_1, t_2, t_3)$ is dominated by coherence transfer efficiency $R_{cte}(\Delta)$ and relaxation $R_2(t_1, t_2, t_3)$.

The MAXY, HSQC, and HMQC methods require coherence transfer between protons and heteronuclei, such as I → S(I) → I or $^1H \rightarrow {}^{13}C(^1H) \rightarrow {}^1H$. The efficiency of such transfer depends on the one-bond coupling constant ($^1J_{SI}$) and the transfer delays (Δ). Effects of long-range coupling constants on $R_{cte}(\Delta)$ are ignored since the values of J_{II} and $^mJ_{SI}$ ($m > 1$) are far smaller than $^1J_{SI}$. For HMQC and HSQC experiments, there are two transfer periods (Δ) and the overall coherence transfer efficiency is proportional to $\sin^2(\pi\, ^1J_{SI}\Delta)$. There are four transfer periods in the MAXY pulse sequences and the efficiency of reaching the maximum-quantum coherence level is proportional to $\sin^{2n}(\pi\, ^1J_{SI}\Delta)$, where n is the number of protons of a CH_n group. The coherence transfer efficiencies calculated over a coupling constant range of 100 to 200 Hz for the different experiments are given in Fig. 4a, where an average coupling constant of 135 Hz is used to set the transfer time [$\Delta = 1/(2\,^1J_{SI})$] and all RF pulses are assumed to have 90° or 180° flip angles. It can be seen from Fig. 4 that the transfer efficiency is reduced when the coupling constants deviate from the average coupling constant. In the MAXY experiment, the coherence transfer efficiency for CH groups shows no difference from those in the HMQC and HSQC experiments, but there is some relative intensity loss for CH_2 and CH_3 groups. However, the $^1J_{SI}$ coupling constants of CH_2 and CH_3 groups are normally in a small range and close to the average value, and thus the coherence transfer efficiency of MAXY is very close to that of HMQC and HSQC experiments.

Other factors that may affect the sensitivity of those methods include homonuclear coupling, spin relaxation, diffusion, and field inhomogeneity. The two extra coherence transfer periods in the MAXY-based experiments require about 7 ms, which is obviously too short for relaxation and diffusion to cause a notable reduction in sensitivity compared with those of HMQC and HSQC experiments. Thus those effects may be ignored. However, cross peaks caused by homonuclear coupling have been observed in the F_1 (MAXY frequency) dimension in a high-resolution 2D MAXY spectrum (*2*), and this can cause line splitting in the F_1 dimension. The homonuclear coupling is also expected in the F_1 dimension of an HMQC spectrum and results in lineshape distortion. However, this is not true for the HSQC experiment, because this only has spin S single-quantum coherence during t_1. On the other hand, geminal couplings are not observable in the MAXY experiment as both spins are involved in their maximum-quantum coherence. This may increase resolution in the F_1 dimension because the geminal coupling constant is generally larger than the coupling constants between vicinal and more distant proton pairs and

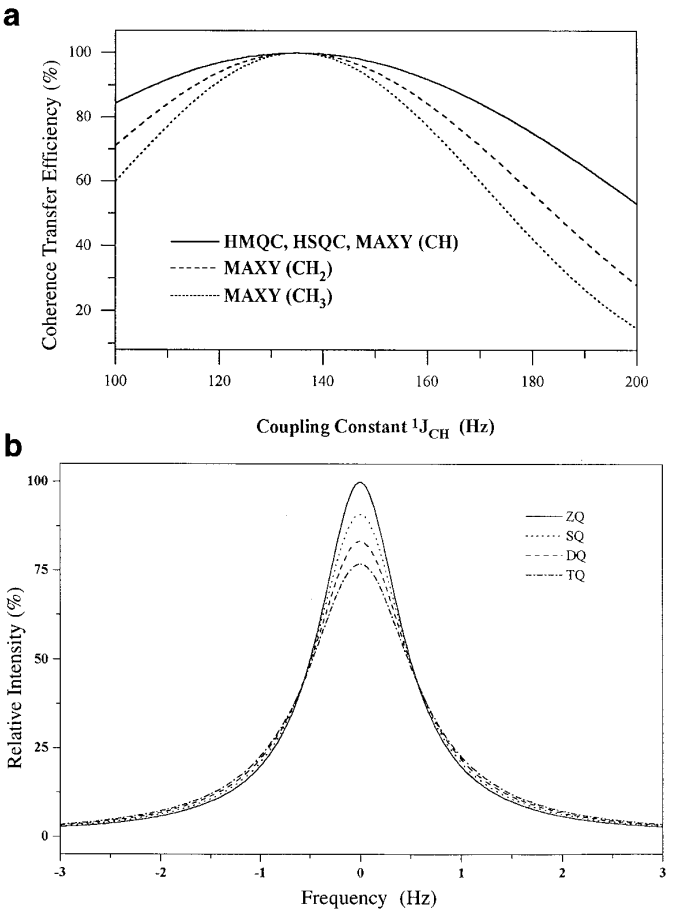

FIG. 4. (a) Plot of the coherence transfer efficiency versus coupling constant value for HMQC, HSQC, and MAXY experiments. A coupling constant ($^1J_{CH}$) of 135 Hz was used to set the transfer delay. (b) Simulation of the effect of magnetic field inhomogeneity on a Lorentzan lineshape and intensity for various quantum orders.

resonance of the CH_2 groups normally appears in the overlapped spectrum region.

The other factor that could cause line broadening is the magnetic field inhomogeneity, which is proportional to the quantum order, the lineshape, $f(\omega)$, and may be described (*28*)

$$f(\omega) = \frac{1/T_2^* + p/T_2^i}{(1/T_2^* + p/T_2^i)^2 + (\omega_0 - \omega)^2}, \qquad [8]$$

where T_2^* is the transverse relaxation time including all contributions with the exception of the field inhomogeneity T_2^i ($\propto 1/\gamma\Delta B$), p is the effective quantum order involved during t_1, and ω_0 and ω are the resonance position and observation frequency, respectively. Figure 4b shows a simulated result with $T_2^* = 2$ s, $T_2^i = 20$ s, and the quantum order (p) from 0 to 3, corresponding to zero quantum (ZQ), single quantum (SQ), double quantum (DQ), and triple quantum (TQ), respectively. The calculated linewidth and relative intensity (maximum peak height) are 0.50 Hz and 100% for ZQ, 0.55 Hz and 91% for SQ, 0.60 Hz and 83% for DQ, and 0.65 Hz and 77% for TQ, respectively. The results indicate that field inhomogeneity has a larger effect on the resonance lineshape and intensity of CH_2 and CH_3 groups in the MAXY-based multidimensional experiments and this is true for all multiple-quantum experiments. The HSQC experiment should have a better response since only heteronuclear single-quantum coherence is involved during t_1. Although the field inhomogeneity line broadening has a larger effect on the sensitivity and resolution in the F_1 dimension for the MAXY experiment than for HMQC and HSQC experiments, this effect can be minimized by probe shimming and good temperature control. Compared with the higher resolution which can be gained from the spin-system separation in the MAXY approach, this line broadening is negligible.

CONCLUSION

A novel three-dimensional pulse sequence, 3D MAXY-HMQC, has been developed and tested using a medium-sized steroid-drug molecule, dexamethasone, in DMSO-d_6. Separation of resonances of CH_n groups is shown to be useful for dispersion enhancement and signal assignment. The effects of coherence transfer efficiency on the sensitivity of the MAXY approach with HMQC- and HSQC-based experiments are compared and the results show that there is no significant sensitivity difference among these methods. The spin system separation shows a higher spectral resolution in the MAXY dimension than HMQC, and this will be of use for the resonance assignment of macromolecules and complex mixtures, including biological samples such as biofluids.

REFERENCES

1. M. Liu, R. D. Farrant, J. K. Nicholson, and J. C. Lindon, *J. Magn. Reson. B* **106,** 270 (1995).
2. M. Liu, R. D. Farrant, J. K. Nicholson, and J. C. Lindon, *J. Magn. Reson. A* **112,** 208 (1995).
3. M. Liu, R. D. Farrant, B. C. Swaetman, J. K. Nicholson, and J. C. Lindon, *J. Magn. Reson. A* **113,** 251 (1995).
4. M. Liu, R. D. Farrant, J. K. Nicholson, and J. C. Lindon, *Magn. Reson. Chem.* **33,** 212 (1995).
5. M. Liu, R. D. Farrant, J. K. Nicholson, J. C. Lindon, P. N. Sanderson, and G. E. Tranter, *Magn. Reson. Chem.* **34,** 865 (1996).
6. D. Marion, P. C. Driscoll, L. E. Kay, P. T. Wingfield, A. Bax, A. M. Gronenborn, and G. M. Clore, *Biochemistry* **28,** 6150 (1989).
7. E. R. P. Zuiderweg, L. P. Mcintosh, F. W. Dahlquist, and S. W. Fesik, *J. Magn. Reson.* **86,** 210 (1990).
8. M. Wittekind, M. Glorlach, M. Friedrichs, G. Dreyfudd, and L. Müller, *Biochemistry* **31,** 6254 (1992).
9. K. L. Constantine, V. Goldfarb, M. Wittekind, J. Anthony, S. C. Ng, and L. Müller, *Biochemistry* **31,** 5033 (1992).
10. W. J. Fairbrother, A. G. Palmer III, M. Rance, J. Seizer, M. H. Saier, and P. E. Wright, *Biochemistry* **31,** 4413 (1992).
11. L. E. Kay, M. Ikura, R. Tschudin, and A. Bax, *J. Magn. Reson.* **89,** 439 (1990).
12. B. T. Farmer II, R. A. Venters, L. D. Spicer, M. G. Wittekind, and L. Müller, *J. Biomol. NMR* **2,** 195 (1992).
13. M. G. Wittekind and L. Müller, *J. Magn. Reson. B* **101,** 201 (1993).
14. R. Weisemann, H. Rüterjans, and W. Bermel, *J. Biomol. NMR* **3,** 113 (1993).
15. L. E. Kay, M. Ikura, and A. Bax, *J. Magn. Reson.* **91,** 84 (1991).
16. A. G. Palmer III, W. J. Fairbrother, P. E. Wright, and M. Rance, *J. Biomol. NMR* **2,** 103 (1992).
17. R. T. Clubb, V. Thanabal, and G. Wagner, *J. Biomol. NMR* **2,** 203 (1992).
18. A. Bax and M. Ikura, *J. Biomol. NMR* **1,** 99 (1991).
19. R. T. Clubb and G. Wagner, *J. Biomol. NMR* **2,** 389 (1992).
20. H. Oschkinat, T. Müller, and T. Dieckmann, *Angew. Chem. Int. Ed. Engl.* **33,** 277 (1994).
21. M. R. Bendall, D. T. Pegg, and D. M. Doddrell, *J. Magn. Reson.* **45,** 8 (1981).
22. G. Bodenhausen and D. J. Ruben, *Chem. Phys. Lett.* **69,** 185 (1980).
23. M. R. Bendall, D. T. Pegg, and D. M. Doddrell, *J. Magn. Reson.* **52,** 81 (1983).
24. A. Bax, R. H. Griffey, and B. L. Hawkins, *J. Magn. Reson.* **55,** 301 (1983).
25. O. W. Sørensen, G. H. Eich, M. H. Levitt, G. Bodenhausen, and R. R. Ernst, *Prog. NMR Spectrosc.* **16,** 163 (1983).
26. G. Bodenhausen, R. L. Vold, and R. R. Vold, *J. Magn. Reson.* **37,** 93 (1980).
27. D. J. States, R. H. Harberkorn, and D. J. Ruben, *J. Magn. Reson.* **48,** 286 (1982).
28. A. A. Bothner-By, R. L. Stephens, J. Lee, C. D. Warren, and R. W. Jeanloz, *J. Am. Chem. Soc.* **106,** 811 (1984).